Effect of Molecular Architecture on Microstructural Characteristics in Some Polysiloxaneimide Multiblock Copolymers

JON SAMSETH,[1] KELL MORTENSEN,[2] JANET L. BURNS,[3] and RICHARD J. SPONTAK[3,*]

[1]Department of Physics, Institute for Energy Technology, Kjeller, Norway, [2]Department of Physics, Risø National Laboratory, Roskilde, Denmark, and [3]Miami Valley Laboratories, The Procter & Gamble Company, Cincinnati, Ohio 45239

SYNOPSIS

Efforts to correlate molecular characteristics with microstructural dimensions in microphase-separated diblock and triblock copolymers have been very successful, resulting in relationships that can be utilized to design materials with a specific microstructure and, consequently, with particular thermomechanical properties. However, similar efforts in the arena of multiblock copolymers have not been nearly as extensive, despite the increasing interest and diversity of this class of materials. In the present work, energy-filtered electron microscopy (EFEM) and small-angle neutron scattering (SANS) are used in a complementary fashion to probe the phase behavior of a series of three polysiloxaneimide (PSI) multiblock copolymers with different molecular architectures. Despite their relatively short segment lengths, all three materials exhibit signs of microphase separation at ambient temperature. SANS data are obtained from chemically unaltered materials and are subsequently interpreted with the Teubner–Strey model for microemulsions. Resultant microstructural dimensions are in good agreement with those measured from EFEM micrographs. Additional insight into the intramolecular sequencing of each copolymer is obtained from scaling relationships.

INTRODUCTION

The numerous experimental studies of block copolymers have proven successful in elucidating the conditions that correspond to the onset of microphase separation (i.e., the weak-interaction limit)[1-5] and in correlating microstructural dimensions with molecular characteristics.[6-11] Most of these efforts have utilized model diblock or triblock systems, typically composed of polystyrene and a polydiene, to ascertain the roles of both the block lengths and residually mixed interphase on bulk thermomechanical properties. Theoretical considerations regarding the initial formation[12,13] and full development[14-20] of microstructural elements in these model systems indicate that the dominant factors in the free-energy function are (i) a measure of the chemical interactions between the blocks (described in terms of a Flory–Huggins χ parameter or a difference in solubility parameters), (ii) the chain length of the copolymer molecule (as given by the degree of polymerization or the equivalent molecular weight), and (iii) the composition of the molecule (expressed in terms of weight or volume fractions). Calculation of the critical conditions corresponding to the microphase-separation transition (MST) in monodisperse diblock copolymers by Leibler[12] has, for instance, provided a sound theoretical basis for understanding the phase behavior of these materials and probing the dynamics of the MST.[21]

Another class of copolymers of equal importance in terms of scientific interest and commercial application is the multiblock, or segmented, copolymer. Materials of this type are normally endowed with

* To whom correspondence should be addressed.

Journal of Applied Polymer Science, Vol. 44, 1245–1256 (1992)
 CCC 0021-8995/92/071245-12$04.00

enhanced mechanical properties due to the presence of microstructural elements in which the dispersed or co-continuous microphases are highly interconnected, as in polyurethane, polyetherester, and polybutadieneamide copolymers. As with the bulk mechanical properties, the phase behavior of these copolymers is also strongly affected by the molecular architecture. Well-defined multiblock copolymers can be designed so that (i) the block lengths are held constant while the chain length and, depending on the architecture, composition vary or (ii) the block lengths are reduced while the chain length and composition are held constant. The latter route better exposes the effect of molecular architecture on microstructural and bulk properties by avoiding complexities arising from the simultaneous variation of two molecular parameters. The caveat associated with this route is that, as the number of blocks increases and the corresponding block lengths decrease, the driving force towards microphase separation is reduced,[22-24] resulting in a greater residually mixed (homogeneous) fraction of material.[24-26] Moreover, specific morphological characteristics (e.g., cubic or lamellar) may change, becoming mixed or distorted, as a phase boundary is crossed or as the degree of molecular interconnectedness imposes severe configurational limitations on individual molecules.

In this work, the phase behavior of three chemically identical polysiloxaneimide (PSI) multiblock copolymers, each possessing relatively short segments but different molecular architectures, is investigated with small-angle neutron scattering (SANS) and energy-filtered electron microscopy (EFEM). Correlations between microstructural dimensions and molecular architecture are proposed on the grounds of scaling principles.

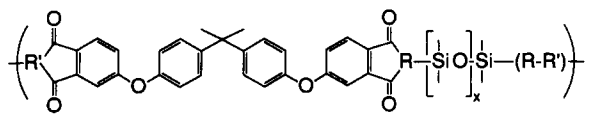

(a)

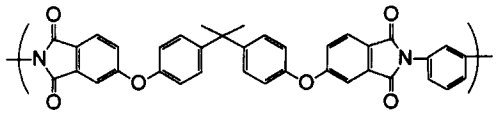

(b)

Figure 1 Chemical structures of the monomers comprising the PSI copolymers used in this study. The "soft" monomer (a) is composed of the reaction product of bisphenol-A (BPA) and a polydimethylsiloxane (PDMS) derivative. Both the degree of polymerization of the PDMS, x, and the reactive end group of the derivative, R, [$=(R - R') + R'$] are proprietary and are not given here. (For additional information on the subject of PSI monomers, the reader is referred to Ref. 25.) The "hard" monomer (b) consists of the product between BPA and m-phenylenediamine, which is the precursor to the ULTEM polyetherimide homopolymer.

Table I Molecular Characteristics of the Copolymers Used in This Study[a]

Designation	w_{PDMS}[b] (%)	N_h[b]	N_s[b]	n_h	n_s
PSI1	37	5.0	4.2	2.3	3.2
PSI2	43	2.8	3.0	2.4	5.2
PSI3[c]	37	Statistical	Statistical	11.6	13.3

[a] Nomenclature defined in text.
[b] Provided by the General Electric Co.
[c] Segment numbers for PSI3 are maximum values based on the assumption of a perfectly alternating monomer sequence.

EXPERIMENTAL

Materials

The materials used in this work have been provided by the General Electric Co. (Waterford, NY) and are composed of the monomers illustrated in Figure 1. The "soft" monomer is the product of bisphenol-A dianhydride with a polydimethylsiloxane (PDMS) derivative, as seen in Figure 1(a). Reaction of the dianhydride with m-phenylenediamine yields the "hard" monomer, which is the precursor for the ULTEM polyetherimide [Fig. 1(b)]. The reactive end group (R) of the PDMS derivative and its degree of polymerization (x) are not provided here due to their proprietary nature but are similar to chemical structures documented elsewhere.[27] All of the copolymers possess number- and weight-average molecular weights of about 25,000 g/mol and 100,000 g/mol, respectively. Examination of Table I reveals that the compositional variation among the three materials is minimal, averaging 37–43 wt % silicone monomer. Distinction among the copolymers arises primarily from the molecular architecture, which is controlled by splitting the dianhydride charge and preparing oligomers of each segment in separate vessels.[28] The number-average degree of polymerization (N) of each segment is also presented for the copolymers in Table I. Unlike the samples designated PSI1 and PSI2, PSI3 is the result of a late-addition reaction and consists of segments whose lengths possess a significant statistical distribution.

It is important to note here the difference between a *segment* and a *block*, as used throughout the remainder of this work. A *segment* refers to the number of like monomers that occur in sequence according to the values of N provided in Table I. A *block*, on the other hand, consists of the number of sequential segments inferred from microstructural characteristics and material balances. Thus, a block may be comprised of a single segment (as in the case of a perfectly alternating multiblock copolymer) or of many segments. These architectures are illustrated in Figure 2. The number of soft segments per copolymer molecule (n_s) can be ascertained from

$$n_s = w_{\mathrm{PDMS}} M / N_s M_{\mathrm{PDMS}} \quad (1)$$

where w_{PDMS} is the weight fraction of the silicone monomer alone (not including the dianhydride part of the soft segment), M is the number-average molecular weight of the molecule, M_{PDMS} is the molecular weight of the silicone monomer, and N_s is the degree of polymerization of the soft segment. The number of hard segments (n_h) is obtained in a similar fashion:

$$n_h = (M - n_s M_s)/M_h \quad (2)$$

where M_s and M_h are the molecular weights of the soft and hard segments, respectively. The values of n_s and n_h tabulated for each material in Table I indicate that PSI1 is able to possess an alternating segment sequence [Fig. 2(a)], while PSI2 is forced to adopt a segment-coupled architecture [Fig. 2(b)]. It should also be noted that the values of n_s and n_h given for PSI3 correspond to the maximum number of segments possible assuming that the monomers are alternating (i.e., N_s and N_h are equal to unity).

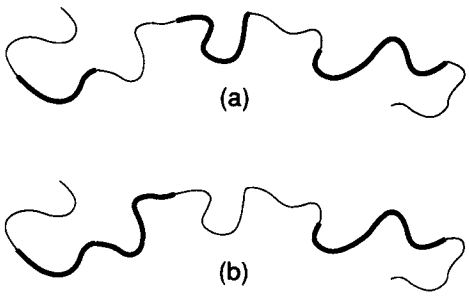

Figure 2 Schematic illustrating the difference between a *segment* and a *block*. A *segment* consists of the number of monomers dictated by the degree of polymerization (N) values tabulated in Table I. The sequence shown in (a) corresponds to a series of perfectly alternating segments, where the light and heavy lines represent the hard and soft segments, respectively. However, depending on the molar composition, not all of the segments must alternate, in which case longer sequences can result in *blocks*, as displayed in (b). Thus, molecules of identical composition and chain length can possess dramatically different molecular architectures (as shown here).

Methods

The three copolymers were received as cut translucent pellets. Samples for electron microscopy were prepared by dissolving pellets in chloroform to produce a 0.5% wt/v solution. These solutions were cast onto clean glass slides and allowed to air-dry. The resultant films were floated off the slides onto deionized water and picked up with 1000 mesh nickel grids, where they were annealed under house vacuum for 15 h at 200°C and then allowed to slow-cool to ambient temperature. Freeze-fracture replicas were obtained by casting the above solution onto the surface of a gold planchette and allowing the solvent to dry until the droplet had flattened, after which a second planchette was immediately placed on top of the tacky film. After further solvent removal (at ambient conditions), the sandwiched film was plunged into liquid ethane (cooled with liquid nitrogen) and fractured in a Balzer's BAF 400T freeze-fracture/etching unit at −170°C. Fracture surfaces were shadowed with platinum at 45° and coated with carbon at 90° for stability. The replicas were subsequently cleaned in chloroform and picked up on 360 mesh copper grids. Both the cast films, measuring on the order of 50 nm thick,[29] and replicas were examined with a Zeiss EM902 electron microscope, operated at 80 keV and equipped with an energy-loss filter to perform EFEM.

Samples measuring 1 mm thick for SANS were produced by melt pressing the as-received pellets at 230°C† for 3 h between clean glass slides and permitting the thick films to cool slowly (−3°C/min) to ambient temperature. No signs of oxidative degradation were observed during this annealing cycle. The films were removed by splitting the slides and carefully peeling off the films. (It should be noted here that PSI1 exhibited the greatest degree of adhesion to the SiO_2 glass.) SANS investigations of these materials were conducted at both Risø National Laboratory and the Institute for Energy Technology. Scattering curves presented in this work were obtained with the ^{3}He-filled detector at Risø National Laboratory. Typical values of the

† This temperature is above the T_g of the hard-segment homopolymer (about 215–225°C[29,30]).

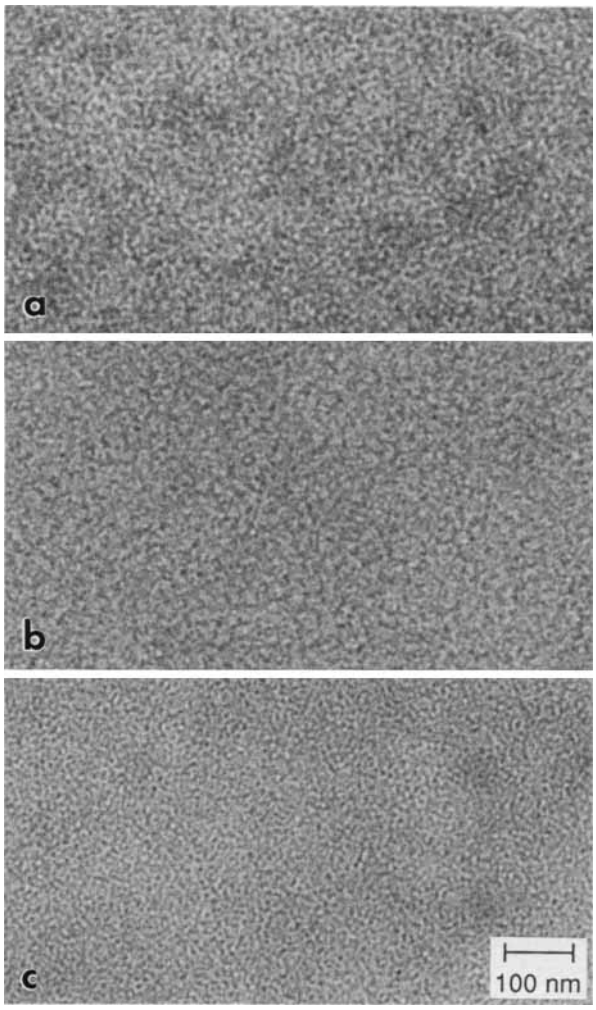

Figure 3 Global bright-field transmission electron microscopy (TEM) images of PSI1 (a), PSI2 (b), and PSI3 (c). A diffuse, mottled texture is present in all of these micrographs, indicating the presence of an established microstructure. Although no staining was required for contrast enhancement between the microphases (because of sufficient electron-density difference), the level of contrast seen in these micrographs remains marginal due to several factors, all of which are discussed in the text.

neutron-beam wavelength were 0.32 and 0.64 nm, and the sample-to-detector distance was varied from 1.0 to 3.6 m.

RESULTS AND DISCUSSION

Electron Microscopy

Typical bright-field electron micrographs of each copolymer are presented in Figure 3. Several features are clear from these micrographs. First, there is a finely mottled texture, indicating the presence of an irregular, but highly networked, microstructure in which the dark regions correspond to the silicone-rich (soft) block. This observation indicates that the copolymers are indeed microphase-separated at ambient temperature. Although trace quantities of residual chloroform are known to exist in the PSI ultrathin films even after annealing,[31] the texture seen in Figure 3 is believed to be representative of the equilibrium microstructure.[32,33] In fact, a freeze-fracture replica of unannealed PSI1, shown in Figure 4, clearly illustrates the presence of this same fine structure, along with a few dispersed chloroform droplets. The second feature to note from Figures 3 and 4 is that, unlike model diblock and triblock copolymers, there is no apparent periodic pattern to the microstructure. This is not surprising in light of the fact that other[29,34–37] multiblock copolymers have also been found to possess morphologies similar to those seen in Figures 3 and 4.

The obscured details apparent in Figures 3(a)–(c) can be attributed to any or all of the following factors: (i) incomplete microphase separation, resulting in a significant residually mixed fraction; (ii) surface segregation of PDMS, responsible for silicone enrichment at the polymer/air and polymer/glass interfaces; or (iii) a high degree of inelastic electron scattering, most likely due to the presence

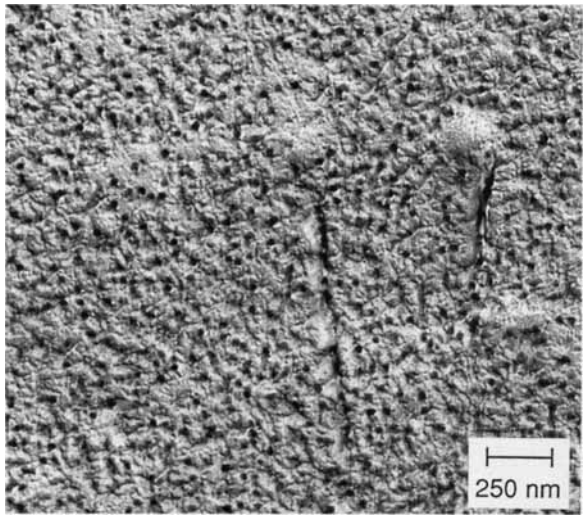

Figure 4 Freeze-fracture replica of PSI1 clearly showing the same morphology seen in Figure 3(a). Unlike model diblock or triblock copolymers, this morphology is irregular, presumably the result of the multiblock architecture.[29,34–37] Residual chloroform, the solvent used in preparing solutions of these materials for film casting, is seen as the large dispersed droplets.

of amorphous carbon. In the case of the first possibility, evaluation of the hard-block glass-transition temperature in each material by dynamic mechanical thermal analysis (DMTA), along with additional SANS results, indicates that the copolymers do possess a nontrivial homogeneous fraction.[38] Little can be done to rectify this thermodynamically favored[24,26] feature inherent in these multiblock copolymers. As for the second possibility, McGrath and co-workers[36,37] have utilized angular-dependent X-ray photoelectron spectroscopy (ADXPS) and electron spectroscopy for chemical analysis (ESCA) to show that the surface concentration of siloxane in several polysiloxanecarbonate and polysiloxanesulfone copolymers is considerably greater than that of the bulk material. This same phenomenon has been observed in a number of different block copolymer systems, always with the component of lower surface energy migrating to the polymer/air or polymer/substrate interface, and is presumed to play a vital role in the development of microstructure seen in Figures 3(a)–(c). This subject will be discussed further in the next section. The last potential source of image degradation—that is, undesirable inelastic-electron scattering—can be virtually eliminated with the use of EFEM, a technique which permits energy-selective filtration of forward-scattered electrons.

Energy-filtered electron microscopy has been used[39–42] extensively in the biological sciences. The principle behind EFEM, illustrated in Figure 5, has been recently discussed by Trinick and Berriman[43] and Reimer and co-workers[44,45] and is briefly described here for the sake of completeness. Electrons are generated from a tungsten filament and proceed to interact with the ultrathin specimen as in the case of conventional transmission electron microscopy (CTEM). However, the forward-scattered electrons passing through the sample film are subjected to an internal magnetic prism/mirror/prism system of the Castaing–Henry–Ottensmeyer[46,47] design, integrated directly into the projector lens. The purpose of this design is to increase the deflection angle of inelastically scattered electrons by converting the dispersion in scattering angle into a dispersion in energy. A window in the resulting energy-loss spectrum can be subsequently chosen for imaging by insertion of a spectrometer slit of width δE just above the image plane (shown in Fig. 5). The slit employed throughout this work is 20 eV.

This configuration permits several novel modes of electron imaging, but only two are utilized in this work—*zero-loss* and *structure-sensitive imaging*. In the former, the energy-loss slit is positioned at the zero-loss peak (corresponding to unscattered and elastically scattered electrons only), thereby rejecting electrons that are inelastically scattered due to plasmon and element-specific interactions. As is evident from the micrographs of PSI1, PSI2, and PSI3 in Figure 6, obtained from similar regions as those shown in Figure 3 and under identical conditions of defocus, the contrast between the microphases is increased significantly. It should be borne in mind that the micrographs in Figures 3 and 6 were produced using identical printing conditions. In structure-sensitive imaging, also referred to as *inelastic dark-field imaging*, micrographs are obtained with inelastically scattered electrons whose energy loss is just below that of the carbon edge ($\Delta E = 284$ eV). Consequently, the image is formed only by electrons inelastically scattered from noncarbonaceous elements. In such images, the microphase comprised primarily of carbon (the imide phase in the present study) appears dark due to the absence of collected electrons, while the silicone-rich microphase is light,

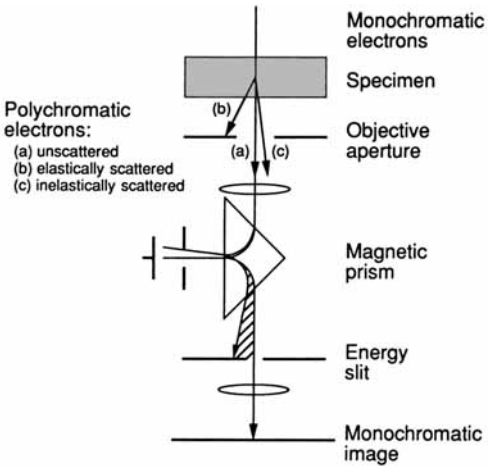

Figure 5 Illustration of energy-filtered electron microscopy (EFEM) with the Zeiss EM902 electron microscope. Electrons transmitted through the sample are categorized as either unscattered, elastically scattered, or inelastically scattered. The first two types of electrons retain their initial energy from the filament source, whereas the latter type exhibits significant energy loss (ΔE). The principle behind the Castaing–Henry–Ottensmeyer[46,47] internal prism design is that the ΔE spectrum can be broadened sufficiently so that inelastically scattered electrons of a particular ΔE value can be accurately filtered through an aperture of predesignated size (δE). In this work, we are concerned with *zero-loss imaging*, which utilizes only electrons that have passed through the specimen without energy loss, and *structure-sensitive imaging*, which use electrons of a particular energy-loss value (namely, $\Delta E \approx 250$ eV).

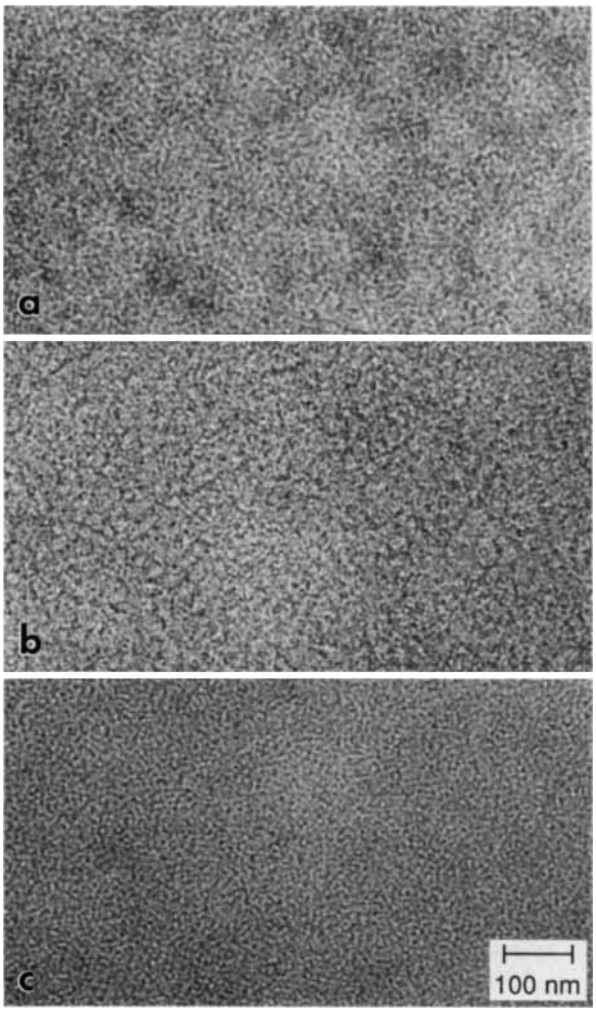

Figure 6 Zero-loss bright-field images of PSI1 (a) PSI2 (b), and PSI3 (c) obtained with EFEM. Note the increased contrast between the microphases (as compared to the images in Fig. 3) due to the removal of extraneous inelastically scattered electrons. The energy window used here is approximately 20 eV. Microstructural dimensions obtained from micrographs such as these are tabulated in Table II.

as seen in a micrograph of PSI2 (Fig. 7). The relatively high fraction of silicon seen in Figure 7 is indicative of either a high degree of microphase intermixing (in agreement with recent[38] SANS results) or surface segregation of PDMS (discussed earlier) or both.

One final point about structure-sensitive imaging that merits mention is the fact that the focal plane is well defined. In bright-field imaging (global or zero-loss), it is possible to increase phase contrast by adjusting the height of the focal plane, thereby resulting in underfocused or overfocused images. However, caution must be exercised with these techniques, as they can produce structural artifacts in conjunction with the contrast-transfer function of the microscope. In dark-field imaging (elastic or inelastic), this potential problem is minimized due to the fact that there is only one focal plane, and any deviation from it results in micrographs of obviously poor quality.

Although these PSI copolymers are not completely microphase-separated (due to their short block lengths), the structure present is most accurately recorded here with EFEM. Microstructural dimensions can then be obtained from contrast-enhanced micrographs, similar to those presented in Figures 6 and 7. Estimates of the characteristic length L_h (e.g., width or diameter) of the dispersed imide-rich microphase, along with the domain periodicity d, are tabulated in Table II. From these values, it is clear that there is significant deviation in the microstructural dimensions obtained from each copolymer, with the mean imide microphase measuring approximately 4.3–7.9 nm thick and the average repeat length ranging from 15.4 to 25.6 nm, depending on molecular architecture. The order of magnitude of the dimensions obtained here are in excellent agreement with that reported[27,29,35–37] for some chemically related copolymers. It is of interest

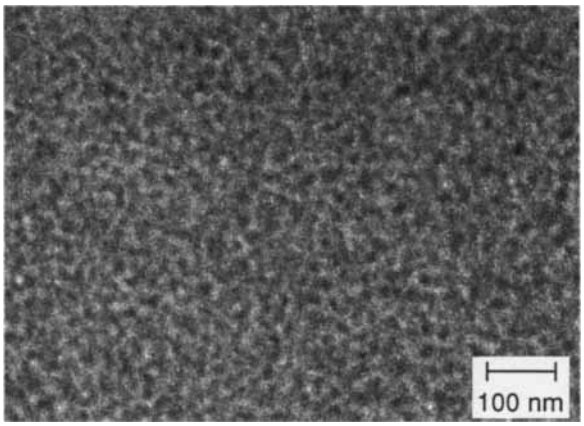

Figure 7 Structure-sensitive EFEM micrograph of PSI2. The image was acquired at an accelerating voltage of 80 keV and an energy-loss value (ΔE) of approximately 250 eV, just below the carbon-loss edge (ΔE = 284 eV). The silicon-rich phase, appearing dark in typical bright-field images, is seen as the bright microphase due to the absence of inelastically scattered electrons from carbon, which appear dark at $\Delta E \approx 250$ eV. As in Figure 6, the energy window used to obtain this micrograph is about 20 eV; but due to the electron optics, the resolution in this imaging mode is slightly lower than that found in Figure 6.

Table II Microstructural Characteristics of the Copolymers Investigated Here[a]

	EFEM		SANS			
Designation	L_h (nm)	d (nm)	q^* (nm^{-1})	d_B (nm)	d_{T-S} (nm)	ξ_{T-S} (nm)
PSI1	6.0	19.7	0.38	16.5	15.0	8.1
PSI2	7.9	25.6	0.27	23.5	21.4	9.0
PSI3	4.3	15.4	≈ 0.34	—	13.1	3.2

[a] Nomenclature defined in text, with the subscripts B and T-S referring to parameters obtained from Bragg's law and the Teubner-Strey[50] model [eqs. (6) and (7)], respectively.

to note that the "randomly coupled" PSI3 possesses the smallest domains and shortest periodicity of all three materials, also in accord with morphological investigations[32] of some polysiloxanecarbonate copolymers.

Small-Angle Neutron Scattering

It must be borne in mind that the irregularity of the microphases, evident in all of the micrographs, hampers the accuracy of such microstructural quantification. Also, as alluded to earlier, segregation of the silicone-rich component to a surface is responsible for a layer whose siloxane concentration is higher than that of the bulk material, thereby influencing the microstructural development in ultrathin films. Small-angle neutron scattering is a powerful complementary technique, used to discern accurate measurements of *average* microstructural dimensions in bulk specimens. The one criterion for obtaining meaningful data from SANS is that the microphases exhibit sufficient neutron-scattering contrast. In most SANS efforts, one microphase, or a portion thereof, is selectively deuterated to increase this contrast. However, block copolymers exhibit some degree of inherent neutron contrast by virtue of the degree of protonation in each block.[‡] The scattering length densities (β) of the monomers depicted in Figure 1 can be calculated from

$$\beta = \frac{1}{V} \sum_i b_i k_i \qquad (3)$$

where b_i is the scattering length of atom i, k_i is the number of i atoms in the monomer, and V is the volume of the monomer. Using values of b_i found in the literature[48] and assuming that the average mass densities of the hard and soft blocks are about 1.17 and 1.03 g/cm^3, respectively,[29] we estimate β for the imide monomer to be about 25×10^{-12} cm/nm^3 and that for the silicone-rich monomer to be approximately 8.3×10^{-12} cm/nm^3.

It is clear from these values that the scattering contrast between microphases is expected to be much lower than in typical diblock and triblock copolymers in which one or more blocks is selectively deuterated. However, scattering patterns for the three copolymers, found in Figure 8, reveal a significant degree of neutron scattering. Both PSI1 [Fig. 8(a)] and PSI2 [Fig. 8(b)] are observed to yield relatively sharp isotropic scattering peaks, while PSI3 [Fig. 8(c)] exhibits a diffuse isotropic peak. These peaks are representative of the dispersed microstructural elements in the materials (as observed with EFEM and CTEM) and are not believed to be related to a "correlation hole."[2,49] Before continuing, it must be pointed out that the emphasis of the subsequent SANS interpretations is on characterizing the microstructure in each copolymer. No attempt is made here to elucidate single chain statistics from these data due to the high degree of polydispersity and the distribution in molar composition inherent in these materials.

Quantification of microstructural dimensions from scattering patterns such as in Figure 8 is accomplished through subtraction of background scattering, followed by normalization with respect to a standard (in this case, water) and circular integration of the pattern. Cross-section scattering spectra ($d\Sigma/d\Omega$) are shown as functions of the scattering vector (q) in Figure 9 for PSI1 and PSI2 and in Figure 10 for PSI3. The scattering vector is defined as

$$q = \frac{4\pi}{\lambda} \sin \frac{\theta}{2} \qquad (4)$$

[‡] The extent of protonation is important as a measure for differentiating the blocks in SANS, since the coherent neutron scattering length for hydrogen is negative whereas those for all the other elements (carbon, silicon, oxygen, and nitrogen) are positive.[48]

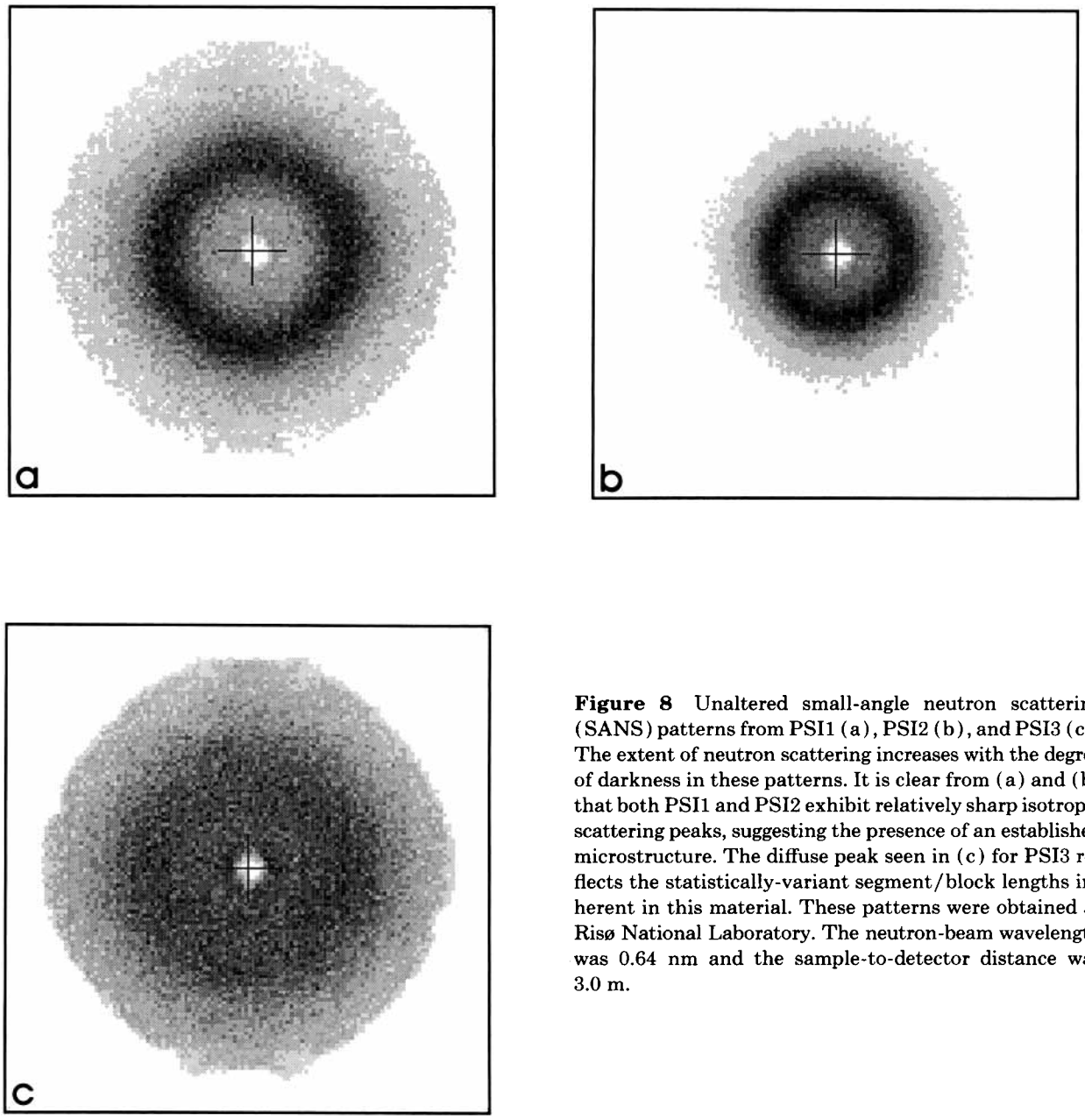

Figure 8 Unaltered small-angle neutron scattering (SANS) patterns from PSI1 (a), PSI2 (b), and PSI3 (c). The extent of neutron scattering increases with the degree of darkness in these patterns. It is clear from (a) and (b) that both PSI1 and PSI2 exhibit relatively sharp isotropic scattering peaks, suggesting the presence of an established microstructure. The diffuse peak seen in (c) for PSI3 reflects the statistically-variant segment/block lengths inherent in this material. These patterns were obtained at Risø National Laboratory. The neutron-beam wavelength was 0.64 nm and the sample-to-detector distance was 3.0 m.

where λ is the wavelength of the neutron beam (0.32 nm in Figs. 9 and 10) and θ is the scattering angle. It is evident from these figures that all three materials exhibit a scattering peak, whose normalized intensity and location depend on the copolymer (or, in other words, on the molecular characteristics). Since both PSI1 and PSI2 are the most blocky of the three materials, they are expected to yield the most distinct peaks (which they do, as seen in Fig. 9). The broad, diffuse peak in the PSI3 spectrum (Fig. 10), on the other hand, is not surprising as it reflects the statistically variant block architecture of the copolymer.

The first microstructural dimension to be deduced from Figure 9 is the microstructural periodicity, which can be estimated from Bragg's law:

$$d = 2\pi/q^* \tag{5}$$

where q^* is the peak position. Values of d corresponding to the relatively sharp peaks in PSI1 and PSI2 are tabulated in Table II. (Due to the breadth of the peak in PSI3, Bragg's law is not rigorously applicable and is not used here for estimation purposes.) Comparison with the mean periodicities obtained from the EFEM micrographs for PSI1 and

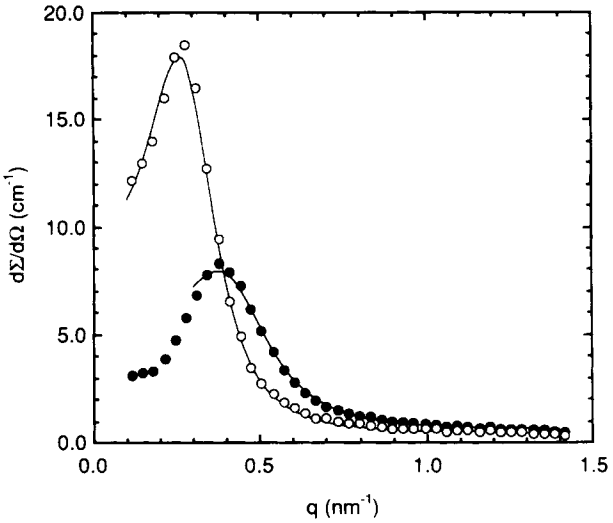

Figure 9 Neutron scattering cross-sections ($d\Sigma/d\Omega$) for PSI1 (●) and PSI2 (○) as functions of the scattering vector q. These spectra, corresponding to patterns in which the neutron-beam wavelength was 0.32 nm and the sample-to-detector distance was 3.6 m, have been corrected for background scattering and have been normalized with respect to water. The differences in peak characteristics between PSI1 and PSI2 are attributable primarily to the difference in molecular architecture. Peak locations are tabulated in Table II, along with corresponding microstructural dimensions inferred from Bragg's law and from the Teubner–Strey[50] scattering model (solid line) for microemulsions.

PSI2 shown earlier (Figs. 3, 6, and 7) indicates good agreement between the results of the two techniques, with values from EFEM being consistently larger. It is of interest to note that the periodicity exhibited by PSI2 is significantly greater than that from PSI1, even though both the soft and hard segments of PSI2 are smaller than those in PSI1 (see Table I). This apparent anomaly will be addressed later.

To ascertain other microstructural dimensions (e.g., microstructural thickness), the normalized data must be fit to some mathematical formalism. After employing several different models, the one emulating the peak characteristics most accurately was the one developed by Teubner and Strey[50] for microemulsions. Here, the postulated density–density correlation function is given by

$$\frac{\langle \rho(0)\rho(r)\rangle}{\langle |\rho|^2\rangle} = \frac{d}{2\pi r} e^{-r/\xi} \sin\left(\frac{2\pi r}{d}\right) \qquad (6)$$

where r is the spatial coordinate and ξ is the correlation length, which provides a characteristic length for the scattering microphase. The Fourier transform of eq. (6) yields the scattering cross section:[51]

$$\frac{d\Sigma(q)}{d\Omega} = 2\pi\psi\left\{\left[\xi^{-2} + \left(\frac{2\pi}{d}\right)^2\right]^2 + 2\left[\xi^{-2} - \left(\frac{2\pi}{d}\right)^2\right]q^2 + q^4\right\}^{-1} \qquad (7)$$

Chen et al.[52] have shown that $\psi = 4\phi_s\phi_h\Delta\beta^2/\xi$, where ϕ_i ($i = s$ or h) is the volume fraction of microphase i and $\Delta\beta^2 = (\beta_h - \beta_s)^2$. The model is based on scattering from microemulsions and therefore relies on the premise that the interface between the dispersed and continuous phases is sharp. This is not the case for these three copolymers, whose scattering behavior in the high-q (Porod's) regime deviates markedly from the q^{-4} dependence required for infinitely thin interfaces, thereby indicating the presence of finite interfacial regions.[10] This aspect of the scattering behavior of these materials is presented elsewhere.[38] However, with this limitation notwithstanding, the scattering peaks are well described by the model fit, which is shown as the solid lines in Figures 9 and 10. Both ξ and d derived from the model for each copolymer are provided in Table II. Comparison of the d values with those obtained from Bragg's law [eq. (6)] and EFEM once again reveals very close

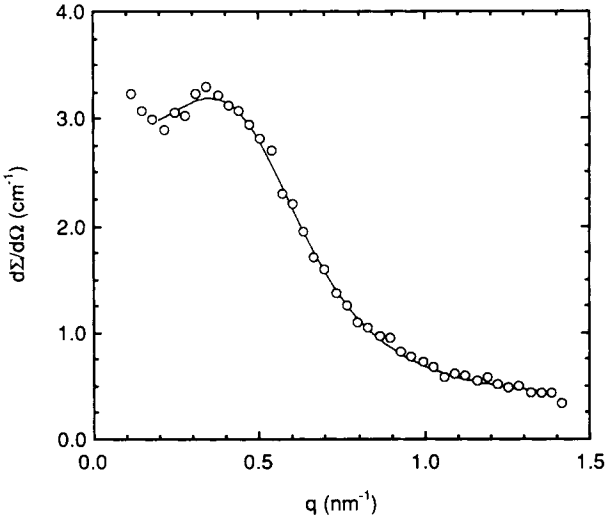

Figure 10 Normalized scattering spectrum from PSI3. The diffuse peak corresponds to the broad-scattering pattern seen in Figure 8(c). Since the sequence of segments/blocks in this copolymer is statistically variant, this type of peak is not surprising as it suggests that the microstructure in this material approaches the limit of microscopic homegeneity (i.e., the disordered state[21,53]). The solid line represents the fit of the Teubner–Strey[50] model.

agreement. It is also of interest to note that the value of ξ calculated for each material agrees well with the thickness of the imide microphase measured from electron micrographs.

Upon close examination of Figure 9, several anomalies appear which warrant explanation. The first is that the scattering peak in PSI2 is sharper than its analogue in PSI1, even though the size of the PSI2 hard segments is smaller than those in PSI1 (see Table I). The second apparent discrepancy relates to the microphase periodicity, as alluded to earlier. In principle, we should be able to use these pieces of information to gain insight into the molecular architecture possessed by these copolymers. If the block configurations in these materials behave as those in diblock and triblock copolymers, then the scaling relationships developed for diblock and triblock copolymers are expected to be applicable to these multiblock systems. For instance, numerous studies, both theoretical[17-19,24] and experimental,[7-9] have shown that the microdomain periodicity in a microphase-separated diblock copolymer scales as

$$d \sim M^{\alpha} \tag{8}$$

where M is the number-average molecular weight of the molecule and α is a scaling parameter commonly reported as $\approx$0.67. The same type of principle is also observed for the characteristic length of the ith block (L_i):

$$L_i \sim M_i^{\alpha} \tag{9}$$

where M_i is the molecular weight of block i and α remains the same as above. If it is assumed that (i) ξ represents L_i for the imide microphase and (ii) eqs. (8) and (9) accurately reflect the molecular scaling relationships of the microphases in the two blocky copolymers (PSI1 and PSI2), then the ratio of observed correlation lengths can be related to the average molecular architecture of each copolymer by

$$\frac{\xi^{(1)}}{\xi^{(2)}} = \left(\frac{M^{(1)}}{M^{(2)}}\right)^{\alpha} = \left(\frac{N_h^{(1)} n_{h,b}^{(1)}}{N_h^{(2)} n_{h,b}^{(2)}}\right)^{\alpha} \tag{10}$$

where $n_{h,b}^{(i)}$ refers to the number of hard segments per block in copolymer i and the superscripts (1) and (2) refer to PSI1 and PSI2, respectively. It is important to review here the concept of forming blocks from segments. We first postulate that not all of the segments in either the PSI1 or PSI2 molecule are perfectly alternating, and indeed this is particularly true in the case of PSI2 where it is not physically possible. Thus, individual segments of the same type can be found next to each other, thereby forming a longer *uninterrupted* block of a particular monomer species. This type of block building from shorter segments has recently been reported for polystyrenesiloxane multiblock copolymers by Feng et al.[26] Knowledge of the block lengths, along with the number of segments/molecule, can subsequently be used to generate the average architecture of the molecule.

Rearrangement of eq. (10) for $n_{h,b}^{(2)}$ yields

$$n_{h,b}^{(2)} = \frac{N_h^{(1)} n_{h,b}^{(1)}}{N_h^{(2)}} \left(\frac{\xi^{(2)}}{\xi^{(1)}}\right)^{1/\alpha} \tag{11}$$

Since both $N_h^{(1)}$ and $N_h^{(2)}$ are known (Table I), along with $\xi^{(1)}$ and $\xi^{(2)}$ (Table II), values of $n_{h,b}^{(2)}$ are determined by varying $n_{h,b}^{(1)}$. Both $n_{h,b}^{(1)}$ and $n_{h,b}^{(2)}$ are bound by upper limits of 2.3 and 2.4, respectively, in which all of the available segments in the molecules constitute a single continuous block. The lower limit on either parameter is unity, since a block must be comprised of at least one segment. Graphical representation of $n_{h,b}^{(2)}(n_{h,b}^{(1)}, \alpha)$ is presented in Figure 11, along with the upper and lower limits corresponding to the material constraints on PSI2 based on the above considerations. It must be remembered

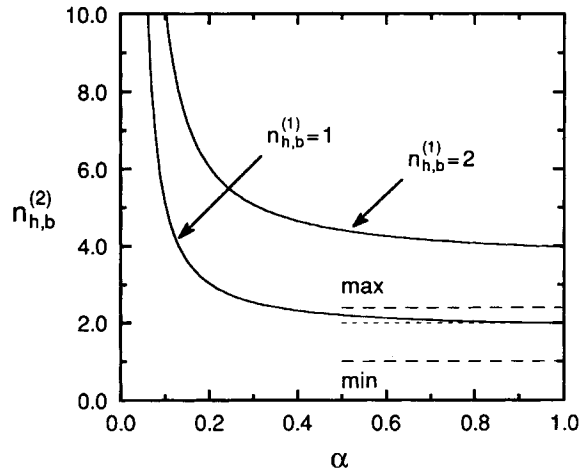

Figure 11 The number of hard segments/block of PSI2 ($n_{h,b}^{(2)}$) as a function of both the number of hard segments/block of PSI1 ($n_{h,b}^{(1)}$) and the scaling variable α, based on eq. (11). The upper (*max*) and lower (*min*) limits on $n_{h,b}^{(2)}$, as dictated by material contraints, are presented as dashed lines. It is clear from this figure that, assuming integral values of $n_{h,b}^{(1)}$, only the $n_{h,b}^{(1)} = 1$ curve is less than the *max* limit of $n_{h,b}^{(2)}$, approaching $n_{h,b}^{(2)} = 2$ (small-dashed line) as $\alpha \rightarrow 1$. This observation strongly suggests that there are two hard segments/block in PSI2 and only one per block in PSI1.

that since the values of N_h provided by the manufacturer and the calculated number of segments/molecule are not integral values, nonintegral values of the number of segments/block are not to be unexpected. To simplify matters at this point, we shall assume that an integral number of segments constitute a single block. Figure 11 clearly shows that only the $n_{h,b}^{(1)} = 1$ curve is less than the upper limit of $n_{h,b}^{(2)}$ over the interval $0.5 \leq \alpha \leq 1.0$ and approaches $n_{h,b}^{(2)} = 2$ as $\alpha \rightarrow 1$. If this observation accurately represents the scaling principles outlined earlier, it is not unreasonable to accept that the mean hard block in PSI1 is composed of a single segment, while that in PSI2 consists of two sequential segments.

This conclusion has several ramifications. First, it would explain why both the imide microphase and domain periodicity in PSI2, as discerned from SANS, are larger than those in PSI1, even though the individual imide segments in PSI1 are longer. Second, it would reveal important information regarding the segment sequences in the copolymer molecules. For instance, using an integral number of segments/molecule, we know that the PSI1 material consists of three soft segments and two hard segments. If the two hard segments are separated (one segment per block), then the only possible architectures permitting this sequence are SHSHS or SSHSH, where S refers to the soft segment and H to the hard segment. Likewise, the molecular architecture of PSI2 with its five soft segments and two hard segments is, according to these arguments, limited to either SSSSSHH (which is not realistic, since this copolymer does not behave like a diblock copolymer in terms of mechanical performance), SSSSHHS, or SSSHHSS. In fact, based on these deductions, PSI2 can be conceptualized as an asymmetric triblock copolymer.

It must be borne in mind that a distribution of molecular architectures is expected in these materials and that precise determination of the number of hard segments per block in either copolymer is actually a moot point. The objective of the preceding analysis has been to demonstrate that, although both materials possess similar compositions and chain lengths, the individual segments in PSI2 tend to form longer sequential blocks than do those in PSI1. This difference in molecular architecture, responsible for the microstructural elements shown here, may help to explain why the mechanical properties of PSI1 differ from those of PSI2.[38]

Analysis of PSI3 in terms of scaling principles is much more difficult since the segments are known to vary statistically in length. For that reason, no attempt is made here to estimate the architecture from the SANS data. However, one point that can be safely made is that the distribution of imide sequence lengths responsible for the diffuse scattering peaks in Figures 8(c) and 10 must be fairly broad and average less than four monomers to produce the calculated correlation length (3.2 nm). This estimate clearly approaches the limit of microscopic homogeneity and the disordered state, as discussed in detail by Hashimoto[21] and Wignall and Bates.[53]

CONCLUSIONS

We have successfully employed energy-filtered electron microscopy (EFEM) and small-angle neutron scattering (SANS) to identify and characterize the microstructure resulting in three microphase-separated polysiloxaneimide multiblock copolymers. EFEM micrographs obtained at the zero-loss peak and at $\Delta E \approx 250$ eV clearly show the presence of an irregular morphology with no apparent periodic pattern. Freeze-fracture replicas provide the same information, indicating that the microstructural elements are not imaging artifacts. SANS patterns also indicate that these materials produce isotropic scattering peaks, whose peak intensity, breadth, and position depend on the molecular architectures of the copolymers. Microstructural dimensions are obtained by fitting the Teubner–Strey model for microemulsions to the SANS peak data. The thickness of the hard (imide) microphase ranges from approximately 3–9 nm, while the microphase periodicity ranges from 13 to 22 nm, in very good agreement with measurements acquired from EFEM micrographs. Molecular architectures in the two blocky copolymers are deduced from scaling the correlation lengths of the imide microphase in each material. The results of this analysis indicate that the segments in PSI2 form longer uninterrupted blocks than do those in PSI1.

The authors would like to thank the General Electric Co. for providing the materials and the Departments of Physics at Risø National Laboratory and the Institute for Energy Technology for the opportunity to use their respective SANS facilities. Two of us express sincere gratitude to the Norwegian Research Council for Science and Humanities (J. S.) and the Royal Norwegian Council for Scientific and Industrial Research (R. J. S., 1989) for postdoctoral fellowships. We also thank Professor Y. Talmon (Technion, Israel) for helpful comments during the preparation of this manuscript.

REFERENCES

1. R.-J. Roe, M. Fishkis, and J. C. Chang, *Macromolecules*, **14**, 1091 (1981).

2. F. S. Bates and M. A. Hartney, *Macromolecules,* **18,** 2478 (1985).
3. W. G. Jung and E. W. Fischer, *Macromol. Chem. Macromol. Symp.,* **16,** 281 (1988).
4. J. N. Owens, I. S. Gancarz, J. T. Koberstein, and T. P. Russell, *Macromolecules,* **22,** 3380 (1989).
5. C. D. Han, D. M. Baek, and J. K. Kim, *Macromolecules,* **23,** 561 (1990).
6. R. Mayer, *Polymer,* **15,** 137 (1974).
7. G. Hadziioannou and A. Skoulios, *Macromolecules,* **15,** 258, 267 (1982).
8. T. Hashimoto, M. Shibayama, and H. Kawai, *Macromolecules,* **13,** 1237 (1980).
9. T. Hashimoto, M. Fujimura, and H. Kawai, *Macromolecules,* **13,** 1660 (1980).
10. R. W. Richards and J. L. Thomason, *Polymer,* **24,** 275, 1089 (1983).
11. G. Hadziioannou, C. Picot, A. Skoulios, M. Ionescu, A. Matthis, R. Duplessix, Y. Gallot, and J. Lingelser, *Macromolecules,* **15,** 263 (1982).
12. L. Leibler, *Macromolecules,* **13,** 1602 (1980).
13. K. M. Hong and J. Noolandi, *Polym. Commun.,* **25,** 265 (1984).
14. D. J. Meier, *J. Polym. Sci. Part C,* **26,** 81 (1969).
15. S. J. Krause, *J. Polym. Sci. Part A-2,* **7,** 249 (1969).
16. D. F. Leary and M. C. Williams, *J. Polym. Sci. Polym. Phys. Ed.,* **11,** 345 (1973).
17. E. Helfand and Z. R. Wassermann, *Macromolecules,* **9,** 879 (1976); **11,** 960 (1978); **13,** 994 (1980).
18. C. P. Henderson and M. C. Williams, *J. Polym. Sci. Polym. Phys. Ed.,* **23,** 1001 (1985).
19. R. J. Spontak, M. C. Williams, and D. A. Agard, *Macromolecules,* **21,** 1377 (1988).
20. D. J. Meier, in *Thermoplastic Elastomers: A Comprehensive Review,* N. R. Legge, G. Holden, and H. E. Schroeder, Eds., Hanser, New York, 1987, Chap. 11.
21. T. Hashimoto, in *Thermoplastic Elastomers: A Comprehensive Review,* N. R. Legge, G. Holden, and H. E. Schroeder, Eds., Hanser, New York, 1987, Chap. 12, Sec. 3.
22. A. C. Balazc, I. C. Sanchez, I. R. Epstein, F. E. Karasz, and W. J. MacKnight, *Macromolecules,* **18,** 2188 (1985).
23. A. C. Balazc, F. E. Karasz, W. J. MacKnight, H. Ueda, and I. C. Sanchez, *Macromolecules,* **18,** 2784 (1985).
24. J. M. Zielinski and R. J. Spontak, *Macromolecules,* to appear.
25. J. A. Miller and S. L. Cooper, in *Thermoplastic Elastomers: A Comprehensive Review,* N. R. Legge, G. Holden and H. E. Schroeder, Eds., Hanser, New York, 1987, Chap. 12, Sec. 4.
26. D. Feng, G. L. Wilkes, and J. V. Crivello, *Polymer,* **30,** 1800 (1989).
27. C. A. Arnold, J. D. Summers, Y. P. Chen, R. H. Bott, D. Chen, and J. E. McGrath, *Polymer,* **30,** 986 (1989).
28. P. R. Wiley, General Electric Co., Waterford, NY, private communications, 1987–88.
29. R. J. Spontak and M. C. Williams, *J. Appl. Polym. Sci.,* **38,** 1607 (1989).
30. I. W. Serfaty, in *Polyimides: Synthesis, Characterization, and Applications,* K. L. Mittal, Ed, Plenum, New York, 1984, Vol. I, pp. 149–161.
31. G. G. Lamprecht and R. J. Spontak, unpublished data obtained with electron energy loss spectroscopy (EELS) and element-specific imaging (ESI) on a Zeiss EM902 electron microscope (1990).
32. R. J. Spontak, J. Samseth, and S. E. Bedford, *Eur. Polym. J.,* **27,** 109 (1991).
33. S.-I. Ogata, H. Maeda, M.-A. Kakimoto, and Y. Imai, *J. Appl. Polym. Sci.,* **33,** 775 (1987).
34. S. K. Varshney and C. L. Beatty, *Am. Chem. Soc. Polym. Prepr.* **22,** 321 (1981).
35. T. C. Ward, D. P. Sheehy, J. S. Riffle, and J. E. McGrath, *Macromolecules,* **14,** 1791 (1981).
36. N. M. Patel, D. W. Dwight, J. L. Hedrick, D. C. Webster, and J. E. McGrath, *Macromolecules,* **21,** 2689 (1988).
37. D. W. Dwight, J. E. McGrath, J. S. Riffle, S. D. Smith, and G. A. York, *J. Electron Spectrosc. Relat. Phenom.,* **52,** 457 (1990).
38. J. Samseth, R. J. Spontak, and K. Mortensen, *J. Polym. Sci., Polym. Phys. Ed.,* to appear.
39. A. L. Arsenault and F. P. Ottensmeyer, *J. Cell. Biol.,* **98,** 911 (1984).
40. D. Frösch, C. Westphal, and R. Bauer, *J. Microsc.,* **147,** 313 (1987).
41. L. D. Peachey, J. P. Heath, G. G. Lamprecht, and R. J. Bauer, *J. Electron Microsc. Tech.,* **6,** 219 (1987).
42. Special issue of *Ultramicroscopy,* **32,** (1990), dedicated to Electron Spectroscopic Imaging and Analysis Techniques.
43. J. Trinick and J. Berriman, *Ultramicroscopy,* **21,** 393 (1987).
44. L. Reimer, I. Fromm, and R. Rennekamp, *Ultramicroscopy,* **24,** 339 (1988).
45. L. Reimer and M. Ross-Messemer, *J. Microsc.,* **155,** 169 (1989); **159,** 143 (1990).
46. R. Castaing and L. Henry, *Acad. Sci. Paris B,* **255,** 76 (1962).
47. F. P. Ottensmeyer and J. W. Andrew, *J. Ultrastruct. Res.,* **72,** 336 (1980).
48. G. D. Wignall, in *Scattering, Deformation and Fracture in Polymers,* G. D. Wignall, B. Crist, T. P. Russell, and E. L. Thomas, Eds., Materials Research Society, Pittsburg, 1987, Vol. 79, pp. 27–45.
49. P.-G. deGennes, *Scaling Concepts in Polymer Physics,* Cornell University Press, Ithaca, NY, 1979, pp. 62–68.
50. M. Teubner and R. Strey, *J. Chem. Phys.,* **87,** 3195 (1987).
51. J. Samseth, S.-H. Chen, J. D. Litster, and J. S. Huang, *J. Appl. Cryst.,* **21,** 835 (1988).
52. S.-H. Chen, S. L. Chang, and R. Strey, *Prog. Colloid Polym. Sci.,* **81,** 30 (1990).
53. G. D. Wignall and F. S. Bates, *MRS Bull.,* **15,** 73 (1990).

Received January 25, 1991
Accepted May 14, 1991